BIOCHEMISTRY
including biophysical chemistry & molecular biology

Article

pubs.acs.org/biochemistry

Nuclear Magnetic Resonance and Molecular Dynamics Simulation of the Interaction between Recognition Protein H7 of the Novel Influenza Virus H7N9 and Glycan Cell Surface Receptors

Eleonora Macchi,[†] Timothy R. Rudd,[‡] Rahul Raman,[§] Ram Sasisekharan,[§] Edwin A. Yates,[∥] Annamaria Naggi,[†] Marco Guerrini,[*,†] and Stefano Elli[*,†]

[†]Istituto di Ricerche Chimiche e Biochimiche "G. Ronzoni", Via Giuseppe Colombo 81, 20133 Milano, Italy

[‡]National Institute for Biological Standards and Control (NIBSC), Blanche Lane, South Mimms, Potters Bar, Hertfordshire EN6 3QG, U.K.

[§]Department of Biological Engineering, Koch Institute of Integrative Cancer Research, Massachusetts Institute of Technology, 77 Massachusetts Avenue, Cambridge, Massachusetts 02139, United States

[∥]Department of Biochemistry, Institute of Integrative Biology, University of Liverpool, Liverpool L69 7ZB, U.K.

Supporting Information

ABSTRACT: Avian influenza A viruses, which can also propagate between humans, present serious pandemic threats, particularly in Asia. The specificity (selectivity) of interactions between the recognition protein hemagglutinin (HA) of the virus capsid and the glycoconjugates of host cells also contributes to the efficient spread of the virus by aerosol between humans. Some avian origin viruses, such as H1N1 (South Carolina 1918), have improved their selectivity for human receptors by mutation in the HA receptor binding site, to generate pandemic viruses. Molecular details and dynamics of glycan−HA interactions are of interest, both in predicting the pandemic potential of a new emerging strain and in searching for new antiviral drugs. Two complementary techniques, ^{1}H saturation transfer difference (^{1}H STD) nuclear magnetic resonance and molecular dynamics (MD) simulation, were applied to analyze the interaction of the new H7 (A/Anhui/1/13 H7N9) with LSTa [Neu5Ac α(2→3) Gal β(1→3) GlcNAc β(1→3) Gal β(1→4) Glc] and LSTc [Neu5Ac α(2→6) Gal β(1→4) GlcNAc β(1→3) Gal β(1→4) Glc] pentasaccharides, models of avian and human receptor glycans. Their interactions with H7 were analyzed for the first time using ^{1}H STD and MD, revealing structural and dynamic behavior that could not be attained from crystal structures, and contributing to glycan−HA specificity. This highlighted aspects that could affect glycan−HA recognition, including the mutation H7 G228S, which increases H2 and H3 specificity for the human receptor. Finally, interactions between LSTc and H7 were compared with those between LSTc and H1 of H1N1 (South Carolina 1918), contributing to our understanding of the recognition ability of HAs.

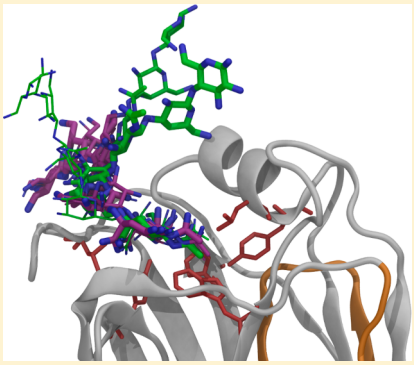

In 2013, a new influenza A subtype was able to diffuse rapidly through the human population in eastern China. Initially, three people in the urban area of Shanghai and Anhui were hospitalized with rapidly progressing lower respiratory tract infections and were found to be infected by the novel avian origin influenza A virus H7N9. This virus showed peculiar properties compared to known similar subtypes, particularly in its propensity to mutate. The transmission of H7 virus rarely involves mammals, while infections of the N9 type viruses in humans had never been observed before.[1] A prerequisite for an avian influenza virus to become pandemic is its ability to be transmitted efficiently in humans by aerosol diffusion, and not to rely on contact between individuals or biological fluids, as was the case for the avian virus infecting birds.[2] The molecular mechanisms by which some animal influenza viruses during their evolution began to propagate in humans have not yet been thoroughly investigated, while this information may prove to be crucial in the design of antiviral drugs and to our ability to predict their pandemic potential. The interaction between the viral capsid protein hemagglutinin (HA) and the glycan receptors on the host cell surface is an important event in the early stage of the infection, which determines the recognition of target cells by the virus,[3] and was shown to be the basis of virus aerosol transmissibility between humans. As an example, the H1N1 virus responsible for the 1918 "Spanish flu" pandemic (SC18, "South Carolina 1918") propagated as efficiently between ferrets by aerosol as it did between humans, but a single mutation (D225G) and a double mutation (D225G/D190E) of amino acids in the H1 receptor binding site (RBS) yielded two artificial viruses, NY18 and AV18, respectively, the former being transmitted inefficiently and the

Received: July 8, 2016
Revised: November 9, 2016
Published: November 9, 2016

DOI: 10.1021/acs.biochem.6b00693
Biochemistry XXXX, XXX, XXX−XXX

latter unable to do so; its lethality and replication activity were preserved.[4] Interestingly, this change in H1N1 virus transmission, correlated with a binding specificity switch of H1, from human to avian glycan receptors. In fact, SC18 binds selectively to the human receptor, NY18 interacts with both human and avian receptors, while the double mutant AV18 binds selectively to the avian receptor.[5] The avian and human receptors are glycan chains "end-capped" by Neu5Ac $\alpha(2-3)$ Gal and Neu5Ac $\alpha(2-6)$ Gal disaccharides, respectively, being frequently found in the intestinal epithelia of birds and on epithelial cells of the upper respiratory tract of humans, these two being the target tissues for avian and human influenza virus infection, respectively.[3] Two model pentasaccharides are commonly used for avian and human glycan receptor, whose primary structure is defined as LSTa [α-D-Neu5Ac (2→3) β-D-Gal (1→3) β-D-GlcNAc (1→3) β-D-Gal (1→4) β-D-Glc] and LSTc [α-D-Neu5Ac (2→6) β-D-Gal (1→4) β-D-GlcNAc-(1→3) β-D-Gal (1→4) β-D-Glc]. Avian and human HAs recognize their receptors through the exposed nonreducing terminal end, characterized by a different conformation and dynamics in solution.[6−8] At the molecular level, the H1 (SC18) specificity switch was explained by observing that the D225G mutation on H1 removed crucial hydrogen bonds between the RBS and the LSTc nonreducing end,[5,8,9] while the additional mutation (D190E) further reduced the extent of contact between its reducing end and the surface of helix 190.[8−10] In contrast, E190 (AV18) was found to interact more efficiently than D190 with Neu5Ac $\alpha(2-3)$ Gal of LSTa, because of its longer side chain,[8] as previously postulated by Gamblin et al.[9] and Srinivasan et al.[5] Other HA subtypes showed changes in their binding specificity following only minor amino acid mutations, including H2 and H3 from H2N2 and H3N2 avian viruses responsible for the pandemic events of 1957 and 1968, respectively. These subtype HAs, through the Q226L and G228S mutations, changed their preference from avian to human receptors.[10] In addition, H7 from H7N9 virus, by analogy with H2 and H3, includes the Q226L mutation[11] in some variants (A/Anhui/1/13), contributing to its affinity for human receptors.[2,12]

In 2013, Xiong et al.[13] compared an avian H7 from H7N3 (A/turkey/Italy/214845/2002) with the human H7 of H7N9 (A/Anhui/1/13), using biolayer interferometry to measure their binding affinity with $\alpha(2-3)$ and $\alpha(2-6)$ sialyl lactosamines. The observed H7s differ by two amino acids, Q226L and G186V, with the human H7 having an affinity comparable to those of both human and avian receptors. In late 2013, an investigation involving two H7 variants isolated from humans, A/Anhui/1/13 (AH-H7N9) and A/Shanghai/1/13 (SH-H7N9), revealed how SH-H7N9, characterized by the "avian signature" Q226, bound the avian receptors preferentially while AH-H7N9, which contained the "human signature" L226, could bind both avian and human receptors with comparable affinity.[14] These results confirmed the weak specificity of this H7 variant for the human and avian receptors.

In this study two complementary techniques, ^{1}H STD NMR and MD simulation were applied for the first time to characterize the interaction between LSTa and LSTc, with H7 (AH-H7N9) in solution, underlining the structural and dynamic properties responsible for the molecular recognition ability of H7, and glycan residues, which cannot be resolved by X-ray diffraction because of the flexibility of the glycan.[2] The pentasaccharides LSTa and LSTc were used as models for avian and human glycan receptors. The same approach was then applied to predict the effect of a single G228S mutation on H7 affinity and binding epitopes toward LSTa and LSTc, a structural biology problem that has been considered only partially in the characterization of this new HA subtype. In fact, considering the similarity of H7 to H2 and H3 subtypes, the selected mutation might have been expected to switch its specificity toward the human receptor (LSTc), pushing the virus to infect humans. Tissue binding tests suggest that H7 affinity improvements can occur to both glycans following mutation, without affecting specificity.[15] The same result was confirmed by glycan microarray and kinetic analysis for H7 of the SH-H7N9 variant[16] and later, during the preparation of this work, by a solid phase binding assay using $\alpha(2-3)$ or $\alpha(2-6)$ sialyl-lactosamines on H7 of AH-H7N9 virus.[17] This mutation was expected to reinforce H7 binding for both glycans, with the hydroxyl moiety of the serine side chains interacting with the sialyl groups of LSTc and LSTa, through the formation of hydrogen bonds. Competitive ^{1}H STD experiments involving an equimolar mixture of LSTc and LSTa interacting with H7sm (H7G228S) qualitatively suggest for H7sm a weak preference for LSTa. In the final part of this paper, LSTc:H7 and LSTc:H1 (H1N1 South Carolina 1918) complexes are compared, using the ^{1}H STD/MD approach. This revealed fundamental structural and dynamic differences between H7 and H1, providing distinct ways to recognize the human receptor LSTc, a comparison that, until now, has not been discussed extensively.

■ MATERIALS AND METHODS

Respiratory Tract Glycan Receptors. The H7 ligands chosen for the ^{1}H STD experiments on H7 and H7sm were pentasaccharide mimetics for avian and human cell surface glycan receptors, whose primary structure is defined as α-D-Neu5Ac (2→6) β-D-Gal (1→4) β-D-GlcNAc (1→3) β-D-Gal (1→4) β-D-Glc for the human receptor (LSTc) and α-D-Neu5Ac (2→3) β-D-Gal (1→3) β-D-GlcNAc (1→3) β-D-Gal (1→4) β-D-Glc for the avian receptor (LSTa). In this work, the residue sequence from the nonreducing (NRE) to reducing end (RE) was labeled a follows: (NRE) Neu5Ac Gal-1 GlcNAc Gal-2 Glc (RE), where "-N" specifies the "Gal" residue numbered sequentially from the NRE. LSTa and LSTc were purchased from Prozyme (Hayward, CA) and Dextra (Reading, U.K.), respectively.

Cloning, Baculovirus Synthesis, and Mammalian Expression and Purification of HA. H7 (AH-H7N9) and the mutated H7sm sequences were codon-optimized for mammalian expression, synthesized with a foldon sequence and six-His tag at the C-terminus (DNA2.0, Menlo Park, CA), and subcloned into a modified pcDNA3.3 vector for expression under the CMV promoter. Recombinant expression of HA was performed in HEK 293-F FreeStyle suspension cells (Invitrogen, Carlsbad, CA) cultured in 293-F FreeStyle Expression Medium (Invitrogen) maintained at 37 °C, 80% humidity, and 8% CO_2. Cells were transfected with polyethyleneimine Max (PEI-MAX, PolySciences, Warrington, PA) with the HA plasmid and were harvested 7 days postinfection. The supernatant was collected by centrifugation, filtered through a 0.45 μm filter system (Nalgene, Rochester, NY), and supplemented with 1:1000 diluted protease inhibitor cocktail (Calbiochem) and supplemented with 1:1000 diluted protease inhibitor cocktail (EMD Millipore). HA was purified from the supernatant using His-trap columns (GE Healthcare) on an AKTA Purifier FPLC system. Eluting fractions containing HA were pooled, concentrated, and buffer exchanged into 1× PBS

DOI: 10.1021/acs.biochem.6b00693
Biochemistry XXXX, XXX, XXX−XXX

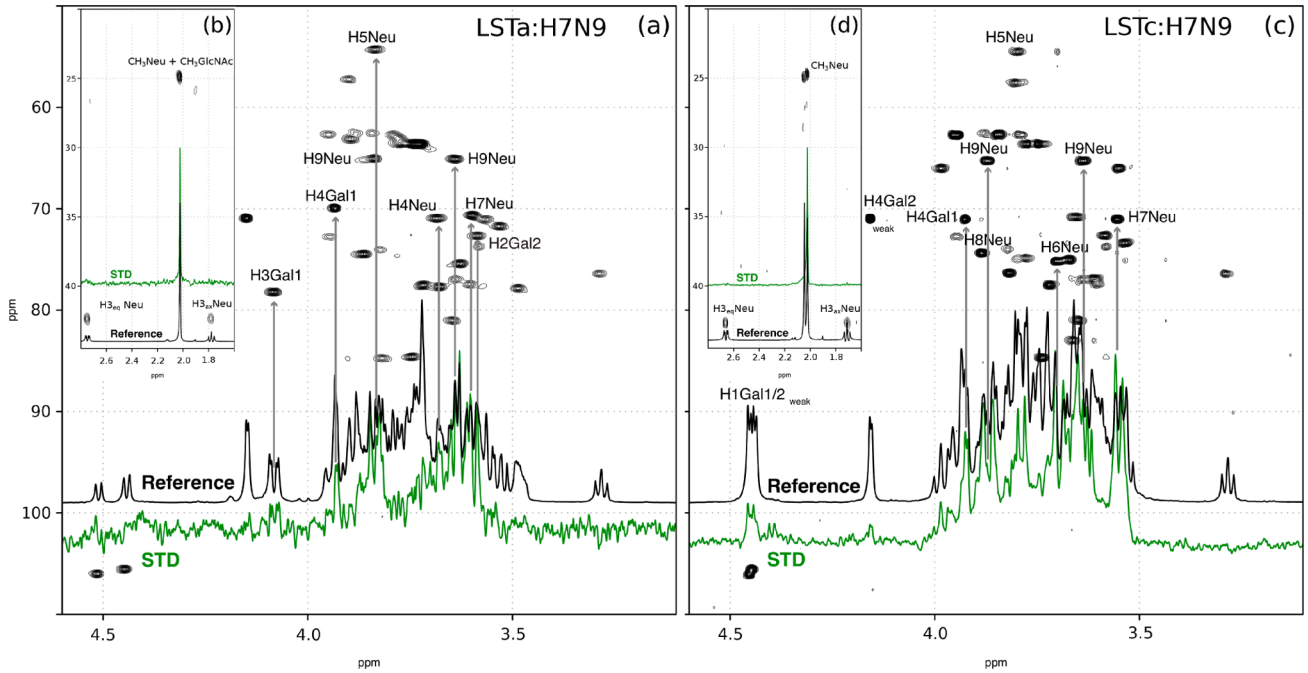

Figure 1. 600 MHz ^{1}H STD NMR spectra of the LSTa:H7 (green lines in panels a and b) and LSTc:H7 (green lines in panels c and d) complexes, superimposed on the corresponding reference spectra (black lines), and on the respective HSQC spectra of LSTa and LSTc. Labels indicate the unequivocally assigned signals. Insets in panels b and d show the *N*-acetyl STD signals of LSTa:H7 and LSTc:H7 receptor complexes, respectively.

(pH 7.4) using 100K molecular weight cutoff spin columns (Millipore, Billerica, MA). The purified protein was quantified using the BCA method (Pierce, Rockford, IL). The recombinant HA was expressed and purified as HA0 and ran as a single band on sodium dodecyl sulfate−polyacrylamide gel electrophoresis. The HA was not cleaved into HA1 and HA2. The HA yield was 1 mg/mL.

NMR Analysis of the Interaction of H7 and H7sm with LSTc and LSTa. ^{1}H STD NMR samples were prepared by washing proteins H7 and H7sm (1 mg/mL) with a buffered solution [150 mM sodium chloride, 100 mM sodium phosphate, 0.3 mM *d*-EDTA, and D_2O (pH 7.2) (Sigma-Aldrich)] using Amicon Ultra centrifugal filters and a 10 kDa membrane (Millipore). Each ligand (LSTc or LSTa) was added to the corresponding protein sample, reaching a final molar ratio of 100:1 (glycan receptor:HA) for the ^{1}H STD measurements. For the competitive experiment, to 200 μg of the first ligand (100:1) was added an additional 200 μg of the second ligand in the NMR tube. The protein concentration for the ^{1}H STD measurements was 0.01 mM. NMR spectra were recorded using Bruker 600 and 900 MHz AVANCE series NMR spectrometers, both equipped with high-sensitivity 5 mm TCI cryoprobes. LSTc and LSTa resonances have been reported by Sassaki et al.[7] For the STD experiments, the on-resonance frequency was set at 7.3 ppm and the off-resonance frequency at 20.0 ppm, a train of 40 Gaussian-shaped pulses of 50 ms each were applied to produce a selective saturation of 2 s, while D1 was set to 6 s. The number of scans was 1K or 2K, and the spectral width was 12626 Hz. The spectra were recorded at 295 K.

Molecular Dynamics Simulations. The interactions between LSTa and LSTc and H7 hemagglutinin (AH-H7N9) and its mutant version, H7sm, were also investigated by comparing the MD simulation trajectories of the following complexes: LSTa:H7 with LSTc:H7 and LSTa:H7sm with LSTc:H7sm. Model complexes LSTa:H7 and LSTc:H7 were built from the corresponding X-ray diffraction structures [Protein Data Bank (PDB) entries 4BSF and 4BSE], where the known conformations of LSTa and LSTc, predicted by Sassaki et al. using the NMR/MD approach,[7] were superimposed on the corresponding $\alpha(2-3)$ and $\alpha(2-6)$ sialyl-lactosamine trisaccharides resolved together with the protein. The glycan:H7 complexes were built to reproduce as much as possible the proper solution environment conformations; in fact, the two glycans in their bound states with H1[8,18] and H3[19] HA were found to be qualitatively similar to their corresponding free states in terms of glycosidic backbone conformation.[7,20] Compared to the nonreducing end disaccharide (Neu5Ac-Gal-1), the minimal root-mean-square distances upon superimposition were 1.53 and 2.92 Å for Neu5Ac and Gal-1, respectively, in the LSTa:H7 complex and 1.12 and 1.93 Å, respectively, measured in the LSTc:H7 complex. In these complexes, only the amino acids forming the H7 RBS structure (from 51 to 251 of 4BSF and 4BSE[13]) were considered. The LSTa:H7sm and LSTc:H7sm complexes were generated from the LSTa:H7 and LSTc:H7 complexes, respectively, by applying a "virtual" mutation, G228S; under this condition, the structure surrounding each ligand was preserved. The LSTc:H1 model complex was prepared using the same approach, but starting from PDB entry 2WRG, including H1 hemagglutinin of H1N1 South Carolina 1918 (SC18), together with four residues of LSTc in H1 RBS, as previously described by Elli et al.[8] Ambertools 1.4[21] was used to build the GLYCAM06[22]/Amber force field for MD simulation of the glycan and protein part of the complexes. The simulation cell was set by enveloping each macromolecule with a water layer (TIP3P[23]) 15 Å wide in the three directions, resulting in an orthogonal cell with edge lengths of approximately 100 Å. The nonbonded potential energy was described using the standard cutoff technique (12 Å) for both electrostatic and dispersive interactions. Each cell was minimized using 100K steps of the default minimization algorithm included in the

DOI: 10.1021/acs.biochem.6b00693
Biochemistry XXXX, XXX, XXX−XXX

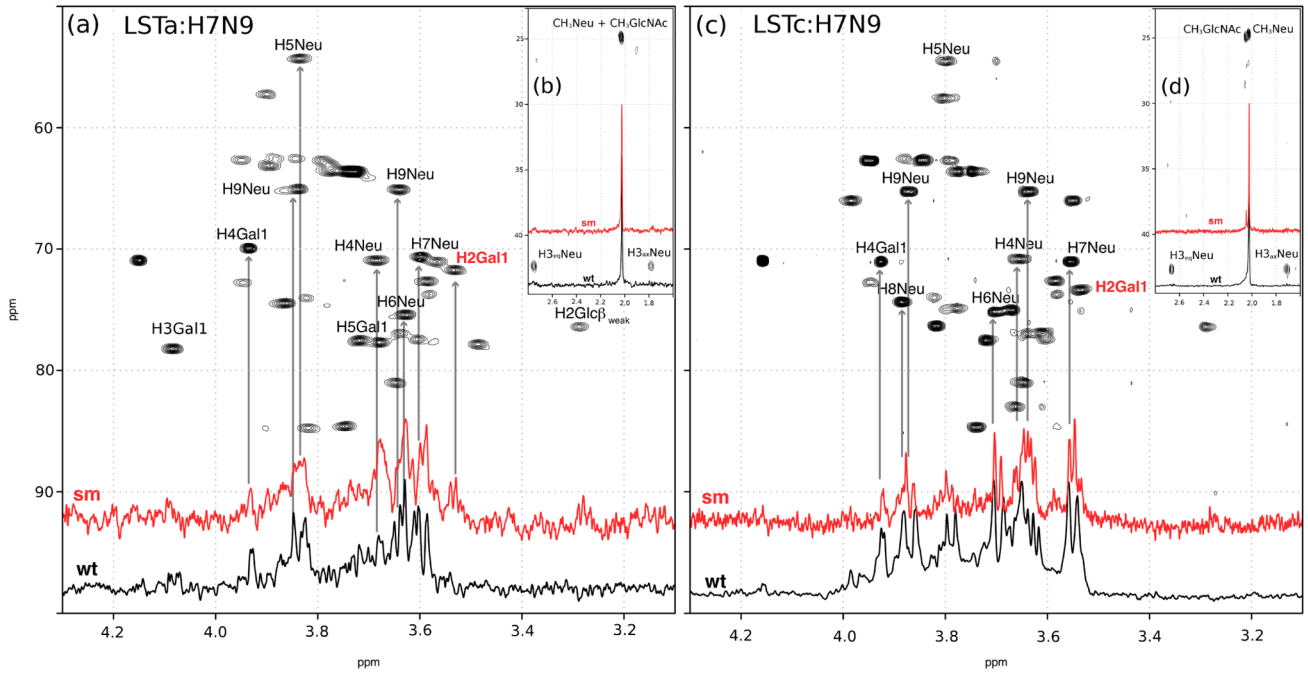

Figure 2. 900 MHz ^{1}H STD NMR spectra of LSTa:H7sm and LSTc:H7sm (red lines in panels a−d) complexes, superimposed on the corresponding ^{1}H STD spectra of LSTa:H7 and LSTc:H7 (black lines) complexes and on the HSQC spectra of LSTa and LSTc. Labels indicate the unequivocally assigned signals. Insets in panels b and d show the *N*-acetyl regions of the overlaid ^{1}H STD HSQC spectra of LSTa:H7sm and LSTc:H7sm receptor complexes, respectively.

NAMD 2.10[24] simulation engine. All the MD simulations were conducted sampling the *NPT* ensemble for the whole length, even if cell density equilibration required approximately 1 ns. The simulation temperature was set at 300 K and maintained by a Langevin thermostat as implemented in NAMD 2.10, while the Nosé−Hoover Langevin piston algorithm controlled the pressure (1.01325 bar) applied on the cell walls. During the minimization and cell density equilibration steps (1 ns), a harmonic potential energy restraint was applied (harmonic constant of 50 kcal mol^{-1}) to all atoms of the complex, while water molecules were allowed to move freely. The MD simulation duration was approximately 150 ns for all cases, and the HA RBS sequence surrounding the glycan (residues 86−101 and 121−224 for H7 and residues 95−110 and 130−233 for H1) was left free to move. Soft harmonic restraints on the HA backbone atoms (Cα, N, and carbonyl carbon) with a harmonic constant of 2.0 kcal mol^{-1} were applied to the remaining sequence, to maintain the secondary and tertiary structure of the HA RBS. The MD simulation trajectory was sampled every 10 ps, and the comparisons between the different complexes were conducted by monitoring selected distances between the ligand and the HA RBS residues, or by images obtained by superimposing snapshots at significant simulation times. This allowed the ligand−HA dynamics to be visualized and the binding state to be compared. The molecular visualization, structural analysis, and MD simulation trajectory analysis were undertaken using VMD 1.9.2.[25] RMSD functions were calculated using the RMSDTT (Root Mean Square Distance Trajectory Tool) plug-in included in VMD 1.9.2. The two-dimensional (2D) histograms of the glycosidic dihedral angles were calculated using R.[26]

■ RESULTS

NMR Analysis of Glycan−HA Interactions. ^{1}H STD experiments allowed the mapping of the ^{1}H-interacting epitope of both human and avian receptors with the tested HAs (the full ^{1}H and ^{13}C assignments of LSTc and LSTa have been published elsewhere[7,8]). The ^{1}H STD spectra of LSTa and LSTc in the bound state with H7 HA were recorded at 600 MHz and are reported in Figure 1 (panels a−d, respectively). The analysis of these spectra revealed that the two glycans interact with H7, primarily through their nonreducing terminal Neu5Ac residue (H4, H5, H7, and H9). In addition to the nonreducing end moiety Neu5Ac, LSTa also interacts with H7 HA through H3 and H4 of Gal-1 and H2 of Gal-2. Unfortunately, because of the overlap of the signals of the CH_3 belonging to Neu5Ac and GlcNAc, it was not possible to resolve which of these groups were involved more closely in the interaction (Figure 1b). Whereas LSTc bound H7 HA using mainly H6−H9 of NeuAc and also H1 and H4 of Gal-1 and Gal-2, these latter STD signals appeared to be weaker than the Neu5Ac resonances (Figure 1c). In this case, it was possible to distinguish between the two methyl groups (Figure 1d). In fact, only the methyl group of Neu5Ac appeared in the ^{1}H STD spectrum of the LSTc:H7 complex, indicating its proximity to the RBS of the protein. This methyl group was likely to be facing toward W153 and the three preserved residues, Y98, H183, and L194, which are located at the bottom of the RBS. The qualitative interpretation of ^{1}H STD NMR spectra of the LSTa:H7 complex showed that the binding epitope is mainly represented by the nonreducing end disaccharide Neu5Ac α(2−3) Gal-1. In contrast for the LSTc:H7 complex, a strong STD signal originating from H2 of Gal-2 suggests the involvement of the LSTa reducing end, certainly Gal-2 and possibly GlcNAc residues, in the binding epitope.

The STD NMR glycan−HA interaction studies were also performed on the single mutant H7G228S (H7sm). The comparison of STD spectra with those obtained with the wild type form of H7 revealed changes in the glycan binding epitopes correlated to the protein mutation (Figure 2). The ^{1}H

DOI: 10.1021/acs.biochem.6b00693
Biochemistry XXXX, XXX, XXX−XXX

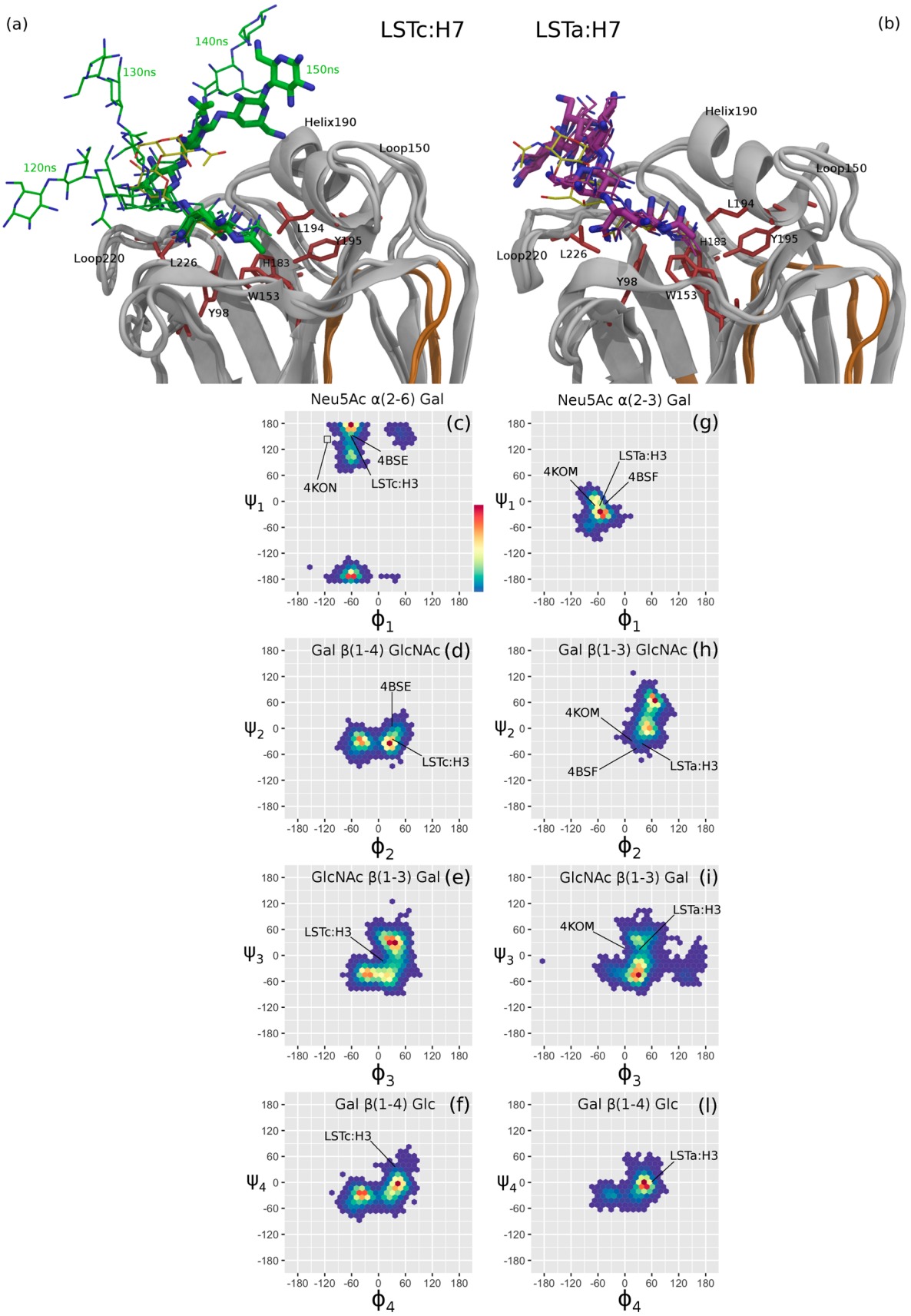

Figure 3. MD-simulated (a) LSTc:H7 and (b) LSTa:H7 complexes at 120, 130, 140, and 150 ns superimposed on the H7 backbone (Cα). The white ribbon shows the H7 amino acid sequence allowed to move freely around the glycan, while the orange ribbon indicates the sequence restrained by a soft harmonic potential applied to the protein backbone. The two ribbons superimposed corresponded to 120 and 150 ns snapshots. The thin yellow tubes represent the X-ray-resolved trisaccharides: Neu5Ac α(2−6) Gal-1 GlcNAc (left) and Neu5Ac α(2−3) Gal-1-GlcNAc (right)

DOI: 10.1021/acs.biochem.6b00693
Biochemistry XXXX, XXX, XXX−XXX

Figure 3. continued

cocrystallized with H7 (H7N9, PDB entries 4BSE and 4BSF). The amino acid residues forming the H7 RBS bottom (Y98, W153, H183, L194, and Y195) and L226 are depicted as red tubes with black labels. Panels c−l show the glycosidic torsional angle maps for LSTc and LSTa in the bound state with H7 sampled by MD simulation; the population is represented by color-coded 2D histograms. Each pair of ϕ_i and ψ_i is split in small but finite elements of area (hexagonal), whose color is proportional to the population of each element (torsional state). This approach localizes the most probable conformations as "clusters" of states (from yellow to red), surrounded by less populated (from cyan to blue). From panel c to l, by graphical inspection, the most probable glycosidic torsional states of the LSTc:H7 and LSTa:H7 complexes are determined with an uncertainty of ≥15°. Dihedral angles of the corresponding glycans determined by Eisen et al.[19] (H3N2), Shi et al.[14] (4KOM and 4KON), and Xiong et al.[13] (4BSE and 4BSF) are indicated by black segments.

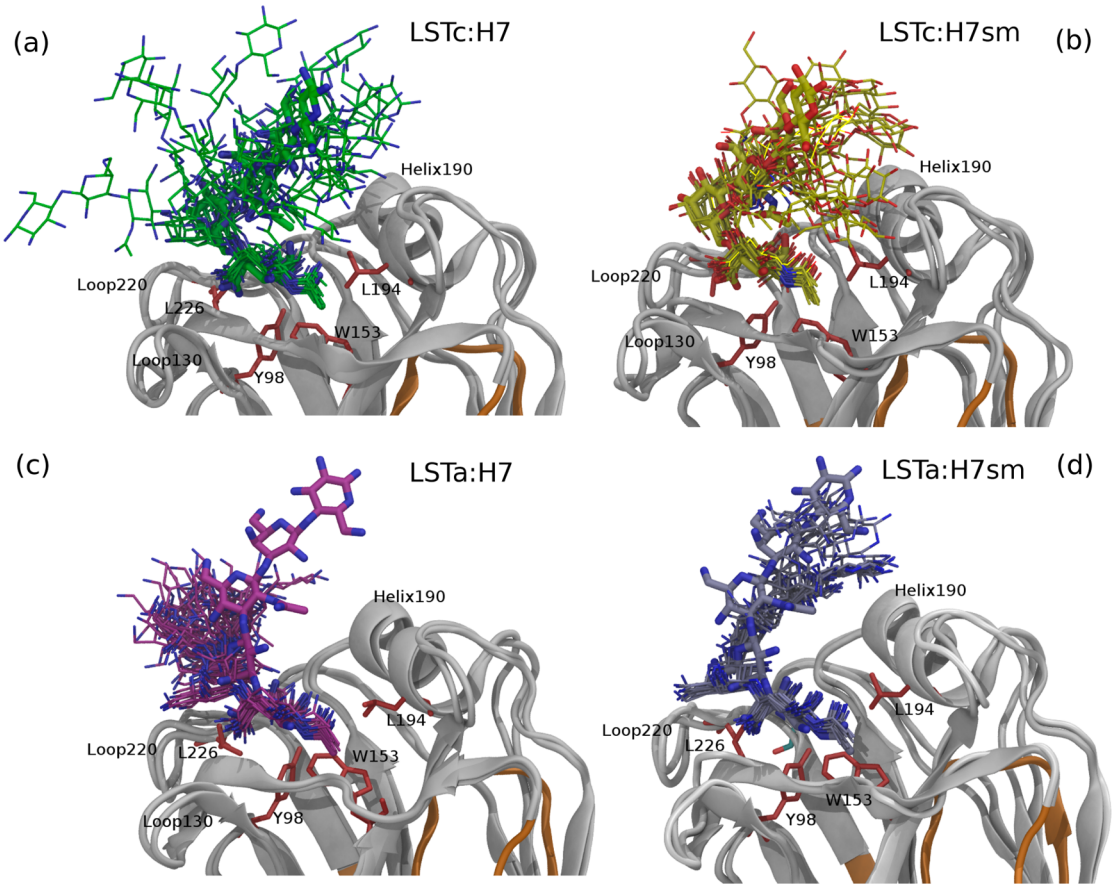

Figure 4. Complexes (a) LSTc:H7, (b) LSTc:H7sm, (c) LSTa:H7, and (d) LSTa:H7sm were reported, superimposing 15 poses of the MD simulation trajectories from 0 to 150 ns sampled in steps of 10 ns. HA was superimposed on its protein backbone (Cα), reported in ribbon representation only for times 0 and 150 ns. The white and orange ribbons correspond to HA sequences free to move and backbone restrained (see Materials and Methods) by soft harmonic potential, respectively. The red tubes and black labels show selected residues of the H7 RBS bottom.

STD spectra of the LSTa:H7sm and LSTa:H7 complexes showed a similar profile (Figure 2a,b), indicating that the interaction involved mainly the Neu5Ac residue, and partially Gal-1 and Gal-2. However, STD signals from H3 and H4 of Gal-1 (weak and medium intensity, respectively) detected in the LSTa:H7 complex were weaker in the LSTa:H7sm complex (H3 of Gal-1 just detected) (Figure 2a). Interestingly, upon H7 mutation, two weak STD signals appeared, H2 Gal-1 and H2 Glc, also indicating the partial involvement of the LSTa reducing end in the interaction. Similar to what was observed with the H7 wild type, the human receptor LSTc interacts with H7sm mainly through the Neu5Ac residues (Figure 2c). In contrast, in the ^{1}H STD spectra of the LSTc:H7sm complex, a weak STD signal belonging to H2 of Gal-1 was detected, while the signal originating from the CH_3 of the GlcNAc (Figure 2d) was weaker in comparison with that of the LSTc:H7 complex, suggesting a weak contact between GlcNAc and H7sm RBS. These results indicated a small but significant difference in terms of binding epitope between the two glycans in the bound state with H7 and H7sm, which is supported qualitatively by the modeling description in the following section.

To qualitatively compare the affinity of LSTa and LSTc for H7sm, a competitive ^{1}H STD experiment was designed in which a sample containing H7sm and an equal amount of LSTa and LSTc glycans were mixed (Figure S1). In the interacting mixture, the ^{1}H STD signals belonging to LSTa in Figure S1 appear slightly stronger than those of LSTc, suggesting that H7sm preferentially binds the avian receptor (LSTa). These results are in accord with the glycan microarray and kinetic results of Yang et al.[16] (compare Figure 2B with Figure 8A, Figure B with Figure 8B, and also Table 5 with Table 6 of Yang et al.). The kinetic, glycan microarray,[16] and solid surface binding[17] assays support an improvement in the affinity of H7 for both human and avian receptor mimetics upon G228S

DOI: 10.1021/acs.biochem.6b00693
Biochemistry XXXX, XXX, XXX−XXX

mutation, even though a weak preference for the avian form could be deduced in glycan microarray and kinetic tests.

Molecular Dynamics Simulation of Complexes of LSTa and LSTc with H7. *MD Simulation and ^{1}H STD Glycan Binding Epitope Comparison.* MD simulations of the glycan−HA complexes were used to adapt the conformation and relative position of binding of LSTa and LSTc to H7, to the water solution environment, and to introduce dynamic aspects of the glycan−HA interaction, complementing the glycan binding epitope mapped by ^{1}H STD spectra. The MD simulation of LSTa:H7 and LSTc:H7 complexes confirmed that Neu5Ac was the primary interacting residue for both glycans (Figure 3a,b). In fact, for the whole simulation (approximately 150 ns), Neu5Ac maintained its starting position at the bottom of H7 RBS, among the conserved residues Y98, W153, H183, L194, and Y195 (H3 numbering), in strict agreement with the corresponding X-ray-resolved three-dimensional (3D) structures,[3,13,14] and with the ^{1}H STD binding epitope. In the LSTc:H7 complex, the RMSDs between Neu5Ac and Gal-1 from their X-ray structures oscillate around values of <1 and 2 Å, respectively (Figure S2, left, black and red lines), while in the LSTa:H7 complex, the corresponding RMSD values fluctuate around 2 Å. The simulated GlcNAc residue show less agreement with the X-ray structure, but if in the LSTc:H7 complex, GlcNAc shows wide fluctuations in RMSD around the average value of 7 Å without convergence, in the LSTa:H7 complex, the RMSD of GlcNAc decreases slowly (Figure S2, green lines). These results support for GlcNAc an interaction weaker than that of LSTc nonreducing end disaccharide, Neu5Ac α(2−6) Gal-1. In contrast, GlcNAc in the LSTa:H7 complex slowly converges to a conformation and relative position approximately 4 Å from the corresponding X-ray structure, suggesting that, in this case, GlcNAc binds H7 RBS with a strength comparable to that of the LSTa nonreducing end residues, Neu5Ac and Gal-1. The Neu5Ac positions in H7 RBS were found to be similar for both LSTa and LSTc, as reported previously for H3 and H5 HA.[19,28] This can be seen in Figure S3 for models of the LSTc:H7 and LSTa:H7 complexes in which the two Neu5Ac residues are superimposed over the protein backbone of hemagglutinin. LSTa showed interaction with H7 RBS employing all its residues from Neu5Ac to Glc, occupying the space between loop 220 and helix 190, corresponding to an unusual binding epitope for an avian-like receptor in the bound state with HA, such as H1, H3, and H5, where the LSTa reducing end protrudes vertically (HA trimer axis) from the RBS.[8,9,19,27,28] MD simulation of the LSTa:H7 complex showed clearly how LSTa left its vertical position (Figure 4c, wide tube) quite early (after ∼30 ns), maintaining its contacts until the end of the MD simulation (Figure 3b). In the LSTa:H7 interaction, the ^{1}H STD binding epitope included recognized signals from Neu5Ac, Gal-1, and Gal-2, while no proton signal belonging to GlcNAc was detected. In another way, the MD simulation description of the LSTa:H7 complex suggests probable contacts between parts of the GlcNAc residue and H7 RBS (loop 220). Overall qualitative agreement between ^{1}H STD basic restraints and the MD-simulated LSTa:H7 could be evinced from Figure 3b. In contrast, the LSTc binding epitope corresponds to Neu5Ac and Gal-1 residues, while the remainder showed longer distances with H7 RBS residues; in fact, the methyl protons of GlcNAc were not seen in ^{1}H STD spectra, in agreement with the conelike surfaces spanned by the LSTc reducing end as predicted by MD simulation (Figures 3a and 4a). This behavior was hypothesized by Chandrasekaran et al.[6] for Neu5Ac α(2−6) Gal-1-terminated glycans longer than three residues but was not observed in the LSTc:H1 complex (SC18) over a comparable simulation time scale, as described below.

Glycosidic Linkage Dihedral Angle Analysis. The Ramachandran plots of the glycosidic linkages of LSTc:H7 and LSTa:H7 complexes sampled by MD simulation are reported in Figure 3c−l. The torsional angle pair of ϕ_1 and ψ_1 correspond to the Neu5Ac Gal-1 glycosidic bond, defined by four consecutive atoms: C1−C2−O6−C6/C2−O6−C6−C5 for LSTc and C1−C2−O3−C3/C2−O3−C3−H3 for LSTa. The remaining pairs of ϕ_i and ψ_i (i = 2 or 4) involve atoms H1−C1−O3−C3/C1−O3−C3−H3 or H1−C1−O4−C4/C1−O4−C4−H4 for each remaining glycosidic junction, including 1→3 or 1→4 connectivity. The ω angle in LSTc is defined by the O6−C6−C5−H5 atoms of the Gal-1 residue. All these dihedral angles are defined in accord with Xu et al.[29] In particular, for the LSTc:H7 complex, the most probable state for ϕ_1 and ψ_1 is a cluster centered at approximately $-60 \pm 180°$ (Figure 3c), where the symbol ± indicates that the angle ψ_1 populates a state characterized by values approaching 180° (trans) from the left and from the right side of this limit. Ramachandran plots of LSTc and LSTa in the bound state with H7 show differences at ϕ_1 and ψ_1 and at ϕ_2 and ψ_2, in the position of the most probable states and the width of their distribution, while ϕ_3 and ψ_3 and ϕ_4 and ψ_4 are comparable. This correlates for both glycans with an asymmetric binding epitope, with stronger contacts at their nonreducing end. The greater degree of conformational freedom of LSTc in the bound state with H7, not observed for LSTa, corresponds to a wider distribution of ψ_1 (Figure 3c,g), while the ω angle contributes to population of two states, located at approximately −54° and ±160°, of which the former is dominant (98%) compared to the latter (2%). Previous structural data for the LSTc:H1[18] and LSTc:H3[19] complexes indicate only a value allowed for ω (−60°), in agreement with the value of −49° measured in MD simulation for the LSTc:H1 complex (SC18). The Ramachandran plots in Figure 3 qualitatively match the dihedral angles determined by X-ray analysis of the corresponding glycans in the bound state with H3 (X31 influenza A, H3N2) by Eisen et al.[19] and H7 (H7N9) by Shi et al.[14] and Xiong et al.[13]

Molecular Dynamics Simulations of Complexes between LSTa or LSTc and H7sm: Effect of the H7G228S Mutation on the Interaction of H7 with the Human or Avian Receptor. MD simulations of the LSTa:H7sm and LSTc:H7sm complexes were compared to those of the previously discussed LSTa:H7 and LSTc:H7 complexes to observe binding epitope and dynamic changes upon H7 mutation (G228S), possibly indicating changes to H7 specificity. The LSTa:H7 and LSTc:H7 model complexes allowed analysis of the H7 RBS at atomic precision, visualizing the way in which the G228S mutation potentially introduces an additional hydrogen bond between H7 RBS and the sialyl tail, C7−C8−C9 of Neu5Ac in both glycans (Figure S4a). Even though, instinctively, this mutation should be expected to reinforce the binding interaction of both glycans at the level of Neu5Ac, possibly correlated to a widening of the H7 RBS,[28] its effects on the glycan binding epitope and on dynamic aspects of the interaction cannot easily be predicted. The possibility of building models of LSTa:H7sm and LSTc:H7sm complexes by "mutating virtually" one amino acid from the previously analyzed LSTa:H7 and LSTc:H7 complexes, leaving the rest

DOI: 10.1021/acs.biochem.6b00693
Biochemistry XXXX, XXX, XXX−XXX

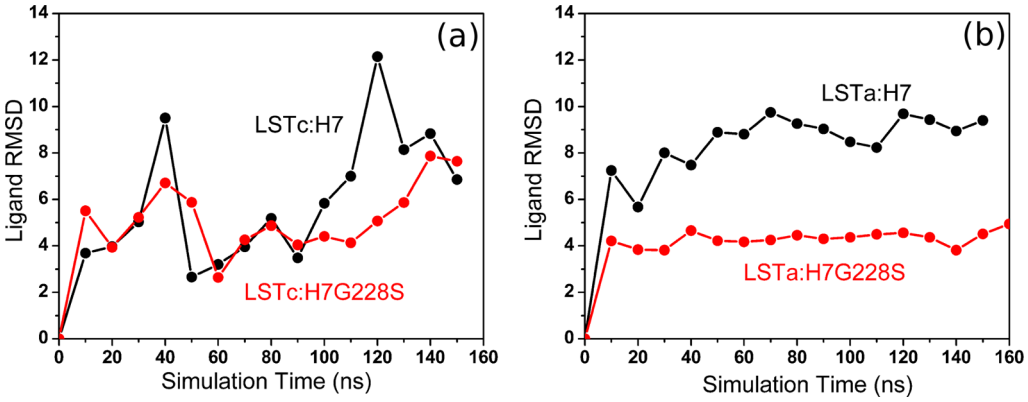

Figure 5. RMSD (root-mean-square distance) of (a) LSTc and (b) LSTa in the bound state with H7 (black) and H7sm (red) at different simulation times using as a reference the ligand conformation at time zero, calculated for the complex structures in Figure 4 after superimposition of the hemagglutinin backbone.

unchanged in both sequence and conformation, allowed significant differences in the MD simulation trajectories to be correlated with the mutation. In particular, LSTa interacting with H7sm showed weak improvement in LSTa reducing end contacts toward the protein, compared to the case for H7. This observation was supported by the distance histograms calculated by MD simulation, exhibiting distances between H2 Glc and protons surrounding the RBS shorter than those of wild type H7 (Figure S4b, right). Similar behavior was observed for the distances between the methyl protons of GlcNAc and the protons surrounding the H7 RBS in the LSTc:H7sm complex, where a greater population of shorter distances was found in comparison to that of the LSTc:H7 complex (Figure S4c, right). This finding was confirmed also by STD experiments, where the STD signal of the methyl group belonging to GlcNAc, not seen in interaction with H7, became weakly visible upon interaction with H7sm, indicating a stronger contact between the LSTc reducing end and helix 190 (Figures 1 and 2d). Similarly, the H2 Gal-1 of LSTc was found closer to the surface of H7sm than H7, as can be observed by the corresponding histograms in the interval between 2.5 and 15 Å (Figure S4c, left).

Via comparison of the MD simulations of the four LSTc:H7sm, LSTc:H7, LSTa:H7sm, and LSTa:H7 complexes, considerable differences between glycan mobility in binding of H7 or H7sm were detected. In the case of LSTc bound to H7sm, a narrower region of conformational space was sampled than for LSTc binding H7 on the same time scale (from 0 to 150 ns), while its nonreducing end disaccharide appeared in both cases to interact with the bottom of the RBS with a greater or comparable strength (Figure 4a,b). Furthermore, LSTa binding H7sm appears to be less mobile at the reducing end, in comparison to the LSTa:H7 complex (Figure 4c,d). For LSTa and LSTc, Neu5Ac appears to be strongly bound to HA RBS in both mutated and unmutated versions. Interestingly, this describes for both LSTc and LSTa how the H7G228S mutation, localized near the glycan nonreducing end, induces a lower mobility at the glycan reducing end (Figure 4). The comparison of ligand mobility in H7 RBS before and after mutation can be described by plotting the "distance" (RMSD) of each ligand pose from their reference (time zero) as a function of time interval, after superimposition of the protein backbone in all the analyzed snapshots (Figure 5). Comparing the estimated slopes and values of the RMSD functions for LSTc and LSTa in the bound state with H7 or H7sm explained how the G228S mutation reduces the mobility for both glycans, even though it was slightly more evident for LSTa. To consider the effects of structure relaxation of the tested complexes on ligand mobility, particularly evident at the beginning of the simulation, Figure S5 reports the RMSD functions calculated for LSTc and LSTa as in Figure 5, but used as a reference the snapshot at 80 ns, corresponding to approximately halfway through the MD trajectories. Interestingly, Figure S5 and Figure 5 suggest how the mobilities of LSTa and LSTc in the bound state with H7sm were smaller in comparison to those of the corresponding complexes that included the wild type form of H7. In conclusion, no indication of a significant switch in H7 preference toward LSTc (human receptor) was observed, in contrast to H2 and H3 subtypes, but in agreement with Young et al.[16] and Schrauwen et al.[17]

The glycosidic torsional angle mobility of LSTa and LSTc in the bound state with H7sm and H7 could be compared, revealing interesting details regarding the distinct ability of H7sm and H7 to bind (constrain) the two glycans. Figure S6 shows how the lower mobility of LSTc binding H7sm compared to H7 was localized at ϕ_1 and ψ_1 torsional angles, corresponding to the nonreducing end disaccharide Neu5Ac $\alpha(2-6)$ Gal-1, as seen by its narrower distribution in Figure S6e. In contrast, LSTa in the bound state with H7sm showed a significantly narrower distribution extending on two angle pairs, ϕ_1 and ψ_1 and ϕ_2 and ψ_2, and distinct torsional states at ϕ_3 and ψ_3, in comparison to the LSTa:H7 complex (Figure S6a−c,e−h). These results confirm stronger binding by H7sm to both glycans, even if LSTa appears to be more restrained than LSTc, agreeing with the ligand mobility analysis using the RMSD function shown above.

Comparison of the Interaction between LSTc with H1 and LSTc with H7 Assessed by ^{1}H STD and MD Simulation: H1 and H7 Exhibit Distinct Modes of Binding to the Human Glycan Receptor. Shi et al.[14] showed strong differences in the binding specificity of the hemagglutinin H1 (CA04-H1N1 A/California/04/2009 H1N1) and H7 (AH-H7N9) toward glycan cell surface receptors: the former being specific for LSTc (human) and the latter showing an ability to bind LSTc and LSTa with similar affinity and corresponding to low specificity. In a previous publication, our group analyzed structurally LSTc and LSTa interacting with H1 (H1N1 South Carolina 1918) and selected mutants.[8] This analysis based on ^{1}H STD NMR and MD simulation provided a structural interpretation of a H1

DOI: 10.1021/acs.biochem.6b00693
Biochemistry XXXX, XXX, XXX−XXX

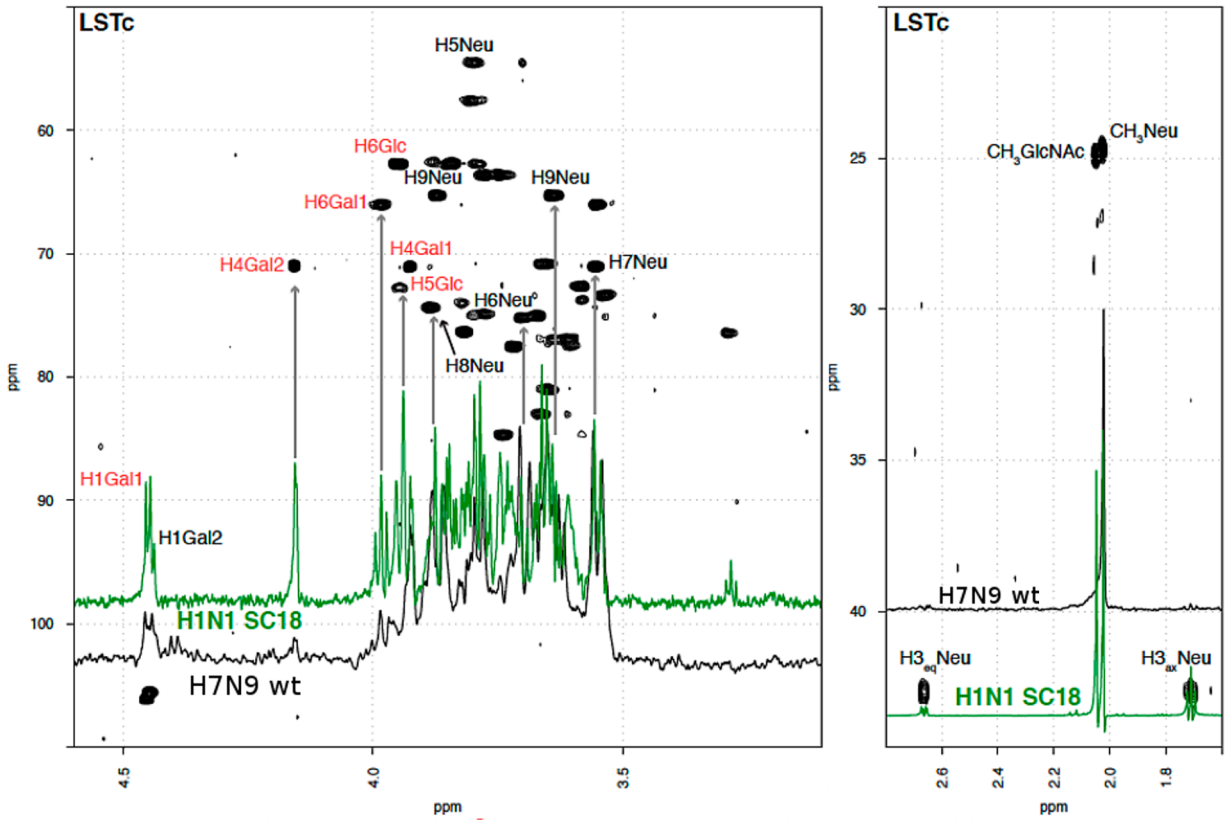

Figure 6. ^{1}H STD spectra of LSTc interacting with H1 (H1N1 SC18) (green) and with H7 (H7N9 A/Anhui/1/13) (black). The STD spectra are superimposed on the 2D HSQC spectra of LSTc (black contour lines). Protons detected through STD are labeled in red for the LSTc:H1 interactions.

specificity switch in LSTc and LSTa driven by H1 RBS mutations. Via comparison of ^{1}H STD spectra of LSTc in the bound state with those of H1 and H7 (Figure 6, green and black lines, respectively), different binding epitopes became visible. LSTc interacts with H7 mainly through Neu5Ac and Gal-1 (H1 and H4), while in the LSTc:H1 interaction, Neu5Ac was the residue of primary interest but the four remaining monosaccharides were also involved: H1 and H4−H6 of Gal-1, CH3 of GlcNAc, H4 of Gal-2, and H5 and H6 of Glc. The greater number of protons belonging to LSTc detected in these spectra in comparison to the number for the LSTc:H7 complex supports qualitatively higher "ligand receptor" affinity in the former case, as measured by Shi et al.[14] using a biochemical test (glycan array). Via comparison of the MD simulation trajectories of LSTc:H1 and LSTc:H7 complexes, some structural features of H1 and H7 RBS could be related to their different LSTc recognition abilities. Figure 7 shows how the LSTc reducing end (Gal-1 GlcNAc Gal-2 Glc) was closer to helix 190 in the LSTc:H1 complex (green tubes and cyan ribbon) than in the LSTc:H7 complex (purple tube and white ribbon), while the Neu5Ac position was comparable in both complexes. This difference in the LSTc binding epitope was mainly related to a longer loop 150, characteristic of H7, which disturbed the short-range interactions between the LSTc reducing end and helix 190 and, hence, supported the weaker binding.[2,13,14] Several residues additionally contribute to the higher affinity of H1 for LSTc, such as D190 (helix 190) and the pair of K222 and D225 (loop 220) in H1, E190, and the pair Q222 of G225 in H7. As described previously by Elli et al.,[8] the fact that D190 has a side chain shorter than that of E190

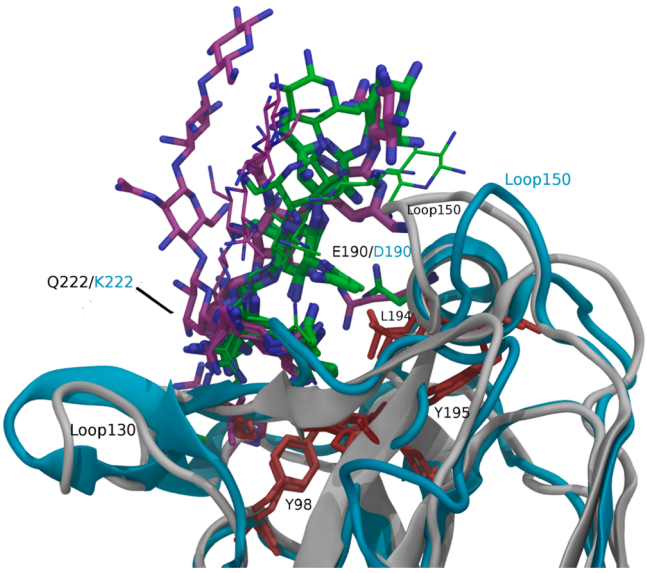

Figure 7. LSTc:H1 and LSTc:H7 complexes represent superimposed snapshots at simulation times of 150 ns of the corresponding MD simulations. LSTc in the bound state with H1 (green tubes for carbon atoms) and LSTc in the bound state with H7 (purple tubes for carbon atoms) at simulation times of 50, 100, and 150 ns are represented by thin, medium, and wide tubes, respectively. H1 and H7 are represented by cyan and white ribbons, respectively, superimposed on the helix 190 protein backbone (Cα). Loop 150, longer in H7 (white ribbon) than in H1 (light blue ribbon), is visible on the top of helix 190.

DOI: 10.1021/acs.biochem.6b00693
Biochemistry XXXX, XXX, XXX−XXX

favored the LSTc reducing end contact with helix 190 (Figure 7 and Figure S7), while the pair of K222 and D225 in H1 bound Gal-1 to loop 220 more strongly than did Q222 and G225 of H7 (Figure S7), considering the possible electrostatic interactions characteristic of the former pair of residues.

The L226 residue, instead of Q226, widens the HA RBS, as observed between the two variants AH-H7N9 and SH-H7N9, having L226 and Q226, respectively.[13,14] MD simulation reproduces an H7 RBS wider and more flexible than H1, visualized by greater distances between loop 130 and loop 220 as reported in Figure S8; these results were also confirmed by the corresponding 3D crystal structure complexes (PDB entries 4BSE and 2WRG). At the bottom of helix 190, the larger hydrophobic V186 (H7) in comparison to P186 (H1) reduces the size of the space to accommodate the Neu5Ac and its sialyl tail (Figure S7c,d), contributing to the larger distances between LSTc and helix 190 when binding H7 and then H1, as observed previously by Xiong et al.[13]

Comparing the glycosidic junction conformation of the LSTc:H7 and LSTc:H1 (SC18) complexes (Figure S9), we find significant differences are located at ϕ_1 and ψ_1 and at ϕ_2 and ψ_2, while ϕ_3 and ψ_3 and ϕ_4 and ψ_4 are more similar. In the LSTc:H7 and LSTc:H1 complexes, ϕ_1 is centered at −60°, but the former complex has a slightly wider distribution, showing a poorly populated state around 60°; ψ_1 has a wider dispersion in the LSTc:H7 complex with a main state centered at ±180° and a secondary state at 90°. At ϕ_2 and ψ_2, the LSTc:H1 complex populates only one state centered at 60°/0° in comparison to the LSTc:H7 complex, where two allowed conformations are located (30°/−30° and −30°/−30°) (Figure S9 and Table S1). Comparing the LSTc:H7 and LSTc:H1 complexes in terms of the number of states and distribution width at ϕ_1 and ψ_1, ϕ_2 and ψ_2, and ω (Figure S9, ω not reported), we find H7 appears to constrain LSTc less efficiently than H1. In fact, for the binding of LSTc to H1, the nonreducing end interaction with the bottom of the HA RBS is reinforced by the interaction between the LSTc reducing end (GlcNAc) and helix 190 (D190, L194), particularly favored by the bent shape of LSTc, as described by Elli et al.[8] The ϕ_1/ψ_1 conformation of the LSTa:H7 complex centered at −60°/−30° is closer to that of LSTa:H1 (NY18) (−60°/0°),[8] LSTa:H3 (−68°/−18°),[19] or LSTa in the free state (−62°/−8°)[7] than to that observed for LSTa:H1 (AV18) (−150°/−30°).[8] These structural and dynamic details indicate a lower affinity of LSTc for H7 than for H1, as observed by Shi et al.[14]

■ DISCUSSION

This work, considering both structural and dynamic aspects, improved our understanding of the molecular mechanisms by which the H7 hemagglutinin of the new influenza A virus H7N9 recognizes human and avian glycan receptors. The combination of experimental NMR spectroscopic techniques and MD simulations used in this study provided structural and dynamic information that cannot be fully revealed by the static X-ray diffraction description, because of the high flexibility of glycans,[2] and cannot be described by a single snapshot image of a glycan−HA complex. The previously incompletely characterized interaction between glycan receptors and wild type H7 (AH-H7N9 variant) and a biologically relevant mutant (G228S), supposed to switch the H2 and H3 preference from avian (LSTa) to human (LSTc) receptors, was studied. The ^{1}H STD/MD approach indicates that LSTa and LSTc interact with H7 using different binding epitopes, even if Neu5Ac occupies exactly the same position in both glycans, as previously observed for other HA subtypes such as H3 and H5.[19,28] In particular, LSTa binds H7 with Neu5Ac, Gal-1, Gal-2, and possibly GlcNAc, adapting its extended shape to the valley between loop 220 and helix 190, a less usual binding epitope for this glycan compared to other subtype HAs, such as H1, H3, and H5,[8,9,19,27,28] in which the reducing end of LSTa emerges from the HA RBS vertically, allowing Gal-1 and GlcNAc to interact with helix 190 (E190). The LSTc binding epitope involves mainly Neu5Ac and Gal-1, although its reducing end (GlcNAc Gal-2 Glc) showed an interaction propensity that was weaker than the binding observed in the LSTc:H1 (SC18) complex in the previous MD simulation study. In fact, LSTc:H7, distinct from LSTc:H1, reproduces the "umbrella-like" conformations over a time scale of 150 ns as proposed by Chandrasekaran et al.,[6] which correspond to an overall wider distribution of the dihedral angles: ϕ_1 and ψ_1, ω, and, ϕ_2 and ψ_2. Particularly for their nonreducing end disaccharide, this description matches the X-ray 3D structures of α(2−3) and α(2−6) lactosamine in complexes with H7[13] used as references throughout the entire MD simulation. The same approaches were applied to predict the ability of LSTa and LSTc to bind the H7G228S mutant, comparing the structural and dynamic properties of the interaction with those of the wild type version of the protein. ^{1}H STD spectra showed a binding epitope slightly different from the corresponding epitope, indicating that the selected mutation does not affect significantly the relative affinity of H7 for one of the two ligands. The comparison of the MD simulation trajectories between the model complexes, LSTa:H7sm, LSTc:H7sm with LSTa:H7, and LSTc:H7, suggests that the G228S mutation allows H7sm to bind both glycans with a strength greater than that of the wild type version of H7, even if this reinforcement appears to be more efficient for LSTa. This result, supported by preliminary ^{1}H STD competition experiments, suggests that the selected mutation does not switch the H7 preference toward the human glycan receptors, in contrast to similar H2 and H3 subtypes, but is in agreement with glycan arrays and kinetic results for H7 of the SH-H7N9 virus[16] and the previously published solid phase binding assays on H7 of the AH-H7N9 variant.[17]

This work allows also the comparison of H1 (SC18) and H7 (AH-H7N9) RBS in the bound state with LSTc, highlighting the structural details that underlie the differences in affinity toward this model of the human receptor. ^{1}H STD showed that H1 binds LSTc using all five residues, while H7 employs only two of the five residues (Neu5Ac and Gal-1). Additionally the glycosidic dihedral angle distribution analysis revealed a lower mobility for LSTc in the bound state with H1 in comparison to that with H7, supporting the greater strength of binding of H1 to this glycan. The structural and dynamic comparison between the RBS of H1 and H7 revealed crucial differences in loop 150, helix 190, and loop 220, possibly explaining their affinity difference toward the human receptor represented by LSTc, previously determined by biochemical assays, and statically by X-ray-based structural investigation.

The application of three complementary approaches, X-ray diffraction, NMR, and MD simulation, to the structural and dynamic characterization of glycan−HA interactions allowed improvements in the comprehension of the molecular mechanisms behind HA recognition events. All these structural and dynamic aspects are important to the design of antiviral drugs targeting HAs but also for predicting those mutations

DOI: 10.1021/acs.biochem.6b00693
Biochemistry XXXX, XXX, XXX−XXX

that could improve HA specificity for human receptors, a factor at the base of the potential pandemic diffusion of an emerging virus.

■ ASSOCIATED CONTENT

Supporting Information

The Supporting Information is available free of charge on the ACS Publications website at DOI: 10.1021/acs.biochem.6b00693.

Supporting ^{1}H STD spectrum, complementary glycan−HA complex structures, proton−proton pair distribution functions, and glycosidic torsional angle maps (Ramachandran plots) sampled during the MD simulations (PDF)

■ AUTHOR INFORMATION

Corresponding Authors

*E-mail: guerrini@ronzoni.it. Phone: +39 02 70641603.
*E-mail: elli@ronzoni.it,. Phone: +39 02 70641642.

ORCID

Stefano Elli: 0000-0003-0686-2480

Funding

The 900 MHz spectra were recorded at the SONNMR Large Scale Facility in Utrecht, which was made possible by the financial support for the Access to Research Infrastructures activity in the seventh Framework Programme of the EC (Contract 261863, EU-NMR). Part of the MD simulations was performed by the "High Performance Computing platforms for scientific computing" ISCRA-SCAI (Super Computing Application and Innovation) at CINECA (Casalecchio di Reno, Bologna, Italy).

Notes

The authors declare no competing financial interest.

■ ACKNOWLEDGMENTS

We are grateful to Utrecht University, SONNMR Large Scale Facility, and Dr. Hans Wienk for technical assistance. We are also grateful to Dr. L. Mauri of Istituto di Ricerche Chimiche e Biochimiche 'G. Ronzoni' for the 2D histogram plots using R statistical software.

■ ABBREVIATIONS

NMR, nuclear magnetic resonance; MD, molecular dynamics; HA, hemagglutinin; NA, neuraminidase; SC18, South Carolina 1918; RBS, receptor binding site; LSTc, α-D-Neu5Ac (2→6) β-D-Gal (1→4) β-D-GlcNAc (1→3) β-D-Gal (1→4) β-D-Glc; LSTa, α-D-Neu5Ac (2→3) β-D-Gal (1→3) β-D-GlcNAc (1→3) β-D-Gal (1→4) β-D-Glc; ^{1}H STD, ^{1}H saturation transfer difference; HSQC, heteronuclear single-quantum coherence; RMSD, root-mean-square distance.

■ REFERENCES

(1) Gao, R., Cao, B., Hu, Y., Feng, Z., Wang, D., et al. (2013) Human Infection with a Novel Avian-Origin Inuenza A (H7N9) Virus. *N. Engl. J. Med. 368*, 1888−1897.

(2) De Graaf, M., and Fouchier, R. A. M. (2014) Role of receptor binding specificity in influenza A virus transmission and pathogenesis. *EMBO J. 33*, 823−841.

(3) Skehel, J. J., and Wiley, D. C. (2000) Receptor binding and membrane fusion in Virus Entry: The influenza Hemgglutinin. *Annu. Rev. Biochem. 69*, 531−569.

(4) Tumpey, T. M., Maines, T. R., Van Hoeven, N., Glaser, L., Solórzano, A., Pappas, C., Cox, N. J., Swayne, D. E., Palese, P. J., Katz, M., and García-Sastre, A. A. (2007) Two Amino Acid Change in the Hemagglutinin of the 1918 Influenza Virus Abolishes Transmission. *Science 315*, 655−659.

(5) Srinivasan, A., Viswanathan, K., Raman, R., Chandrasekaran, A., Raguram, S., Tumpey, T. M., Sasisekharan, V., and Sasisekharan, R. (2008) Quantitative biochemical rationale for differences in transmissibility of 1918 pandemic influenza A viruses. *Proc. Natl. Acad. Sci. U. S. A. 105*, 2800−2805.

(6) Chandrasekaran, A., Srinivasan, A., Raman, R., Viswanathan, K., Raguram, S., Tumpey, T. M., Sasisekharan, V., and Sasisekharan, R. (2008) Glycan topology determines human adaptation of avian H5N1 virus hemagglutinin. *Nat. Biotechnol. 26*, 107−113.

(7) Sassaki, G. L., Elli, S., Rudd, T. R., Macchi, E., Yates, E. A., Naggi, A., Shriver, Z., Raman, R., Sasisekharan, R., Torri, G., and Guerrini, M. (2013) Human (α2→6) and avian (α2→3) sialylated receptors of influenza A virus show distinct conformations and dynamics in solution. *Biochemistry 52*, 7217−7230.

(8) Elli, S., Macchi, E., Rudd, T. R., Raman, R., Sassaki, G. L., Viswanathan, K., Yates, E. A., Shriver, Z., Naggi, A., Torri, G., Sasisekharan, R., and Guerrini, M. (2014) Insights into Human Glycan Receptor conformation of 1918 Pandemic Hemagglutinin-Glycan Complexes derived from NMR and MD studies. *Biochemistry 53*, 4122−4135.

(9) Gamblin, S. J., Haire, L. F., Russell, R. J., Stevens, D. J., Xiao, B., Ha, Y., Vasisht, N., Steinhauer, D. A., Daniels, R. S., Elliot, A., Wiley, D. C., and Skehel, J. J. (2004) The Structure and Receptor Binding Properties of the 1918 Influenza Hemagglutinin. *Science 303*, 1838−1842.

(10) Matrosovich, M., Tuzikov, A., Bovin, N., Gambaryan, A., Klimov, A., Castrucci, M., Donatelli, I., and Kawaoka, Y. (2000) Early Alterations of the Receptor-Binding Properties of H1, H2, and H3 Avian Influenza Virus Hemagglutinins after Their Introduction into Mammals. *J. of Virol. 74*, 8502−8512.

(11) Kageyama, T., Fujisaki, S., Takashita, E., Xu, H., Yamada, S., Uchida, Y., Neumann, G., Saito, T., Kawaoka, Y., and Tashiro, M. (2013) Genetic analysis of novel avian A(H7N9) influenza viruses isolated from patients in China, February to April 2013. *Euro Surveillance 18*, 20453.

(12) Srinivasan, K., Raman, R., Jayaraman, A., Viswanathan, K., and Sasisekharan, R. (2013) Quantitative Description of Glycan-Receptor Binding of Influenza A Virus H7 Hemagglutinin. *PLoS One 8* (2), e49597.

(13) Xiong, X., Martin, S. R., Haire, L. F., Wharton, S., Daniels, R. S., Bennett, M. S., McCauley, J. W., Collins, P. J., Walker, P., Skehel, J. J., and Gamblin, S. J. (2013) Receptor binding by an H7N9 influenza virus from humans. *Nature 499*, 496−9.

(14) Shi, Y., Zhang, W., Wang, F., Qi, J., Wu, Y., Song, H., Gao, F., Bi, Zhang, Y., Fan, Z., Qin, C., Sun, H., Liu, J., Haywood, J., Liu, W., Gong, W., Wang, D., Shu, Y., Wang, Y., Yan, J., and Gao, G. F. (2013) Structures and Receptor Binding of Hemagglutinins from Human-Infecting H7N9 Influenza Viruses. *Science 342*, 243−247.

(15) Tharakaraman, K., Jayaraman, A., Raman, R., Viswanathan, K., Stebbins, N. W., Johnson, D., Shriver, Z., Sasisekharan, V., and Sasisekharan, R. (2013) Glycan Receptor Binding of the Influenza A Virus H7N9 Hemagglutinin. *Cell 153*, 1486−1493.

(16) Yang, H., Carney, P. J., Chang, J. C., Villanueva, J. M., and Stevens, J. (2013) Structural Analysis of the Hemagglutinin from the Recent 2013 H7N9 Influenza Virus. *J. Virol. 87*, 12433−12446.

(17) Schrauwen, E. J. A., Richard, M., Burke, D. F., Rimmelzwaan, G. F., Herfst, S., and Fouchier, R. A. M. (2016) Amino Acid Substitutions That Affect Receptor Binding and Stability of the Hemagglutinin of Influenza A/H7N9 Virus. *J. Virol. 90*, 3794−3799.

(18) Kadirvelraj, R., Grant, O. C., Goldstein, I. J., Winter, H. C., Tateno, H., Fadda, E., and Woods, R. J. (2011) Structure and binding analysis of Polyporus squamosus lectin in complex with the Neu5Acα2−6Galβ1−4GlcNAc human-type influenza receptor. *Glycobiology 21*, 973−984.

DOI: 10.1021/acs.biochem.6b00693
Biochemistry XXXX, XXX, XXX−XXX

(19) Eisen, M. B., Sabesan, S., Skehel, J. J., and Wiley, D. C. (1997) Binding of the Influenza A Virus to Cell-Surface Receptors: Structures of Five Hemagglutinin−Sialyloligosaccharide Complexes Determined by X-Ray Crystallography. *Virology 232*, 19−31.

(20) Sabesan, S., Bock, K., and Paulson, J. C. (1991) Conformational analysis of sialyloligosaccharides. *Carbohydr. Res. 218*, 27−54.

(21) Case, D. A., Darden, T. A., Cheatham, T. E., III, Simmerling, C. L., Wang, J., Duke, R. E., Luo, R., Walker, R. C., Zhang, W., Merz, K. M., Roberts, B. P., Wang, B., Hayik, S., Roitberg, A., Seabra, G., Kolossvai, I., Wong, K. F., Paesani, F., Vanicek, J., Liu, J., Wu, X., Brozell, S. R., Steinbrecher, T., Gohlke, H., Cai, Q., Ye, J., Wang, J., Hsieh, M.-J., Cui, G., Roe, D. R., Mathews, D. H., Seetin, M. G., Sagui, C., Babin, V., Luchko, T., Gusarov, S., Kovalenko, A., and Kollman, P. A. (2010) *AMBER 11*, University of California, San Francisco.

(22) Kirschner, K. N., Yongye, A. B., Tschampel, S. M., González-Outeiriño, J., Daniels, C. R., Foley, B. L., and Woods, R. J. (2008) GLYCAM06: A Generalizable Biomolecular Force Field. Carbohydrates. *J. Comput. Chem. 29*, 622−655.

(23) Jorgensen, W. L., Chandrasekhar, J., Madura, J. D., Impey, R. W., and Klein, M. L. (1983) Comparison of simple potential functions for simulating liquid water. *J. Chem. Phys. 79*, 926−935.

(24) Phillips, J. C., Braun, R., Wang, W., Gumbart, J., Tajkhorshid, E., Villa, E., Chipot, C., Skeel, R. D., Kale, L., and Schulten, K. (2005) Scalable molecular dynamics with NAMD. *J. Comput. Chem. 26*, 1781−1802.

(25) Humphrey, W., Dalke, A., and Schulten, K. (1996) VMD: Visual molecular dynamics. *J. Mol. Graphics 14*, 27−38.

(26) R Development Core Team (2008) *R: A language and environment for statistical computing*, R Foundation for Statistical Computing, Vienna.

(27) Liu, J., Stevens, D. J., Haire, L. F., Walker, P. A., Coombs, P. J., Russell, R. J., Gamblin, S. J., and Skehel, J. J. (2009) Structures of receptor complexes formed by hemagglutinins from the Asian Influenza pandemic of 1957. *Proc. Natl. Acad. Sci. U. S. A. 106*, 17175−17180.

(28) Ha, Y., Stevens, D. J., Skehel, J. J., and Wiley, D. C. (2001) X-ray structures of H5 avian virus hemgglutininsbound 1 receptor analogs. *Proc. Natl. Acad. Sci. U. S. A. 98*, 11181−11186.

(29) Xu, D., Newhouse, E. I., Amaro, R. E., Pao, H. C., Cheng, L. S., Markwick, P. R., McCammon, J. A., Li, W. W., and Arzberger, P. W. (2009) Distinct glycan topology for avian and human sialopentasaccharide receptor analogues upon binding different hemagglutinins: A molecular dynamics perspective. *J. Mol. Biol. 387*, 465−491.

DOI: 10.1021/acs.biochem.6b00693
Biochemistry XXXX, XXX, XXX−XXX